CrossMark

ORIGINAL PAPER

Nanocomposite polyazomethine/reduced graphene oxide with enhanced conductivity

Sergei Kostromin[1] · Natalya Saprykina[1] · Elena Vlasova[1] · Daniel Țîmpu[2] ·
Vasile Cozan[2] · Sergei Bronnikov[1]

Abstract We produced thermally reduced graphene oxide (rGO) by reduction of graphene oxide using a thermal shock followed by annealing at 800 °C. The PAZ/rGO nanocomposite comprised of conjugated azomethine polymer (PAZ) and rGO (2 wt%) was fabricated through solution blending method. Both PAZ/rGO nanocomposite and its components, PAZ and rGO, were investigated with wide-angle X-ray scattering, scanning electron microscopy, transmittance electron microscopy, and atomic force microscopy, Fourier transform infrared spectroscopy, UV-Vis spectroscopy, broadband dielectric spectrometry, four-probe conductivity method, and energy dispersive spectroscopy. Strong physical interaction rather than chemical one between the polymer matrix and rGO nanoparticles was found. Electrical conductivity of PAZ/rGO nanocomposite was detected to increase for four orders as compared with that of pure PAZ.

Keywords Reduced graphene oxide · Polyazomethine · Nanocomposites · Electrical conductivity

Introduction

Nowadays, polymer-based nanocomposites attract much attention because of their superior functional properties, which could be achieved even at small loading with nanoparticles [1, 2]. Among others, carbon nanoparticles, such as carbon black, thermally expanded graphite, fullerenes and their derivatives, single- and multiwall carbon nanotubes, were found to be effective fillers for polymer nanocomposites due to their unique electrical, optical, thermal, mechanical, and chemical properties [3–6]. Since discovery of graphene, which exhibits a two-dimensional monolayer structure, comprised of sp^2-hybridized carbon atoms, arranged in hexagonal lattice [7], it became one of the most promising carbon nanofiller. Graphene demonstrates exceptional physical and chemical properties, such as high thermal conductivity, specific surface aria, excellent electron mobility, high Young's modulus, very high light transmittance, gas impermeability, and chemical stability [3, 7]. These characteristics allow utilizing graphene and its derivatives for production of a wide range of materials and using them as fillers for nanocomposites [3, 7, 8].

The general methods of graphene fabrication are mechanical milling of graphite flakes, electrochemical exfoliation of graphite, and graphene oxide (GO) reduction. Mechanical and electrochemical treatments of graphite are quite effective methods but they need much time and great energy consumption. That is why, thermal, chemical, and electrochemical reduction of GO seem to be more attractive methods of graphene production [7, 9, 10]. Since GO is obtained through graphite flakes treatment with aggressive oxidizing agents for better exfoliation, initially it contains a great number of oxygen-containing functional groups (hydroxyl, carboxyl, epoxide, and carbonyl) and some amount of intercalated water on its surface. Therefore it exhibits a low intrinsic conductivity [7]. In order to decrease quantity of oxygen-containing groups and to enhance intrinsic conductivity of GO, it should rather be reduced. Depending on particular reduction method and the reduction value, it is possible to produce either completely reduced graphene oxide (rGO) or partially reduced graphene

✉ Sergei Kostromin
  k-serg-v@mail.ru

[1] Russian Academy of Science, Institute of Macromolecular Compounds, Bolshoi Prospekt 31, St. Petersburg, Russian Federation 199004

[2] Romanian Academy, "Petru Poni" Institute of Macromolecular Chemistry, Aleea Grigore Ghica Voda 41 A, 700487 Lași, Romania

oxide (prGO). Yet, for chemical reduction of GO, hazardous dangerous chemicals, including hydrazine hydrate, hydroiodic acid, and sodium borohydride are necessary. Therefore this method seems to be undesirable. Oppositely, thermal reduction of GO is sufficiently safe, effective, and easy method. Thermal reduction could be realized either by thermal processing (annealing) in a furnace or under microwave irradiation [7].

There are three basic methods of both polymer/GO and polymer/rGO nanocomposites fabrication: in situ polymerization, melt intercalation, and solution mixing [7]. Much conventional polymers have already been used for producing nanocomposites with graphene and its derivatives: epoxy resins, poly(vinyl alcohol), cellulose, polyurethane, polyaniline, poly(vinylidene fluoride), polycarbonate, poly(ethylene terephthalate), polyamides, polystyrene, alginate, and others [7, 11–13]. Polymer nanocomposites, even at low rGO loading, usually exhibit enhanced properties, such as mechanical strength, thermal stability, and electrical conductivity.

For last ten years, conductive nanocomposites based on conjugated polymers have attracted a great attention, especially as materials for opto-electronics, non-linear optics, and photovoltaics. Originally, conjugated polymers are very weak semiconductors or insulators. However, presence of even a small amount of nanoscaled carbon particles, such as OG or rGO, in polymer matrix may considerably enhance its electro- and photoconductivity [14]. Particularly, polyaniline is one of well-known and sufficiently studied conjugated polymers. It has relatively high conductivity and thermal stability; it could be easily synthesized and it has an ability to change its properties under the influence of protonation/deprotonation. Nevertheless, polyaniline has several disadvantages that limit appreciably possibility of its practical application. They are: poor film- and fiber-forming properties, low mechanical strength, and chemical stability (properties degradation). Therefore, to improve polyaniline properties, polyaniline-based nanocomposites, including composites with GO, have been fabricated [15–18].

Polyazomethines seem to be alternative conjugated polymers [19–21]. Originally, polyazomethines are insulators. However, when they are loaded with conductive nanoparticles, their conductivity tends to arise, while they still keep their mechanical strength, thermal stability, and film- and fiber-forming properties [19].

Previously, we have investigated electrical conductivity of polyazomethine/fullerene C_{60} nanocomposites using a broadband dielectric spectroscopy (BDS) [22, 23]. We have revealed enhanced conductivity of the polyazomethine/C_{60} nanocomposite with 2.5 wt.% of fullerene C_{60} loading. The goals of the present work are production of rGO by thermal shock reduction and fabrication conductive polyazomethine/rGO nanocomposites followed by their investigation with a set of methods. Besides, it could be worth to compare conductivity of polyazomethine-based nanocomposites containing either two-dimensional (2-D) rGO nanoparticles or zero-dimensional (0-D) C_{60} nanoparticles at the same loading.

Experimental section

Materials

As a matrix of polymer nanocomposite, we used a side-chain alkyl-substituted polyazomethine (PAZ). Its chemical structure is shown in Fig. 1. Its principal characteristics are as follows: number-average molecular weight $M_n = 1800$ g/mol, weight-average molecular weight $M_w = 2000$ g/mol, and polydispersity index $PI = 1.12$. Details of its synthesis and other characteristics are available in Refs. [21, 24].

Graphene oxide (GO), as a raw nanofiller material, was produced from graphite powder using a Hummers method originally described in Ref. [25]. Graphite powder (particle size <20 μm) was purchased from Sigma-Aldrich and used as received.

Sample preparation

Fabrication of rGO

For thermally induced GO reduction, we put a portion of diluted aqueous GO dispersion (~6 ml) into a ceramic crucible and dried it at 80–90 °C for 4–5 h. After water evaporation, a thin non-uniform GO film was deposited on the bottom of the crucible. To prevent further rGO flakes scattering, we closed the crucible with a cover. Then we heated a muffle furnace up to 800 °C and put the crucible with GO rapidly into the furnace. In a short time (~20 s) due to the thermal shock, a micro-explosion occurred and the GO film converted into fine-dispersed rGO flakes because of GO exfoliation. In addition, for rGO annealing, the crucible was kept in the furnace at 800 °C for 2 min. In order to use obtained rGO as filler for the polymer matrix, it should be dispersed in an appropriate solvent and the coarse rGO nanoparticles should be removed. For these reasons, we moistened rGO with a small amount of dimethylformamide (DMF), moved it from the crucible into a 50 ml cone flask, added 15–20 ml of DMF, and subjected the mixture to sonication for 3 h followed by its centrifugation for 20 min at 4000 rpm. After centrifugation, stable rGO dispersion in DMF with 0.445 mg/ml concentration was obtained.

Fabrication of PAZ/rGO nanocomposites

To fabricate the PAZ/rGO nanocomposite, we first prepared a PAZ solution. We put 100 mg of PAZ into a 10 ml flask, added 5 ml of DMF, and sonicated the blend at 40–50 °C for 30 min. Then we put the PAZ solution into a 25 ml flask and mixed it with a preliminary calculated volume of rGO dispersion to

Fig. 1 Chemical structure of PAZ
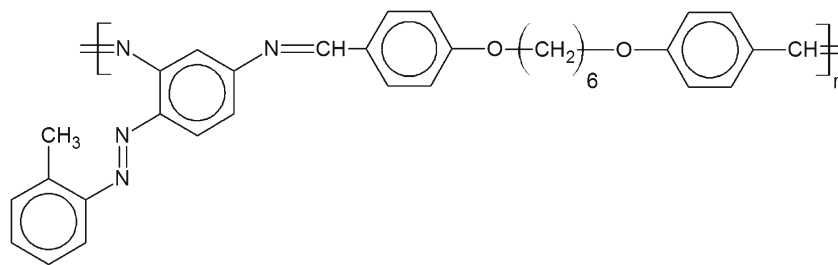
obtain required rGO concentration in the polymer matrix (2 wt%). According to literature data [7, 26, 27] and our experience [22, 23], a chosen rGO concentration was expected to provide sufficient electrical conductivity of PAZ/rGO nanocomposite. Particularly, Yin et al. [27] investigated conductivity of the nanocomposites based on poly(butylene terephthalate) and different types of carbon nanoparticles, including carbon blacks, rGO, and multi-walled carbon nanotubes. They revealed approximate equality of nanocomposites conductivities at 2 wt% of the carbon nanofillers loading irrespectively of the nanoparticle type, though the percolation threshold of the nanocomposites was found to change significantly depending on the nanoparticles type.

We revealed that DMF was the most suitable solvent for preparing both polymer solution and rGO dispersion. Yet, as far as DMF has a high boiling temperature (153 °C), it could difficultly be removed from solution. So for DMF removal, the mixture of PAZ solution and rGO dispersion was subjected to vacuum distillation followed by additional vacuum drying of PAZ/rGO nanocomposite at 60 °C for 24 h.

Methods of investigation

Fourier transform infrared (FTIR) spectra of GO, rGO, PAZ, and PAZ/rGO nanocomposite were performed using a Vertex 70 IR spectrometer (Bruker, Germany) in either transmission regime (in mixture with KBr) or in reflection regime in the range of 4000–500 cm^{-1}.

Ultraviolet-visible (UV-Vis) spectra were recorded with a SF-2000 UV-spectrophotometer (LOMO, St. Petersburg, Russia) in the range of 200–700 nm. We investigated both diluted water dispersions of GO and rGO, and solutions of PAZ and PAZ/rGO nanocomposite in DMF.

Wide-angle X-ray scattering (WAXS) investigations were carried out with a D8 ADVANCE diffractometer (Bruker, Germany, 1.542 Å Cu K$_\alpha$).

The scanning microscopic data were obtained using a Supra 55VP scanning electron microscope (Zeiss, Germany). Both low-temperature cleaved cross-sections of the samples of PAZ and PAZ/rGO composite and rGO particles precipitated on a glass substrate from their dispersion in DMF were investigated. An X-Max energy dispersive detector (Oxford Instrument,

UK) was used for elemental analysis of GO and rGO with energy dispersive spectroscopy (EDS) method.

Transmission electron microscopy (TEM) analysis was performed with a Hitachi HT7700 microscope operated in a high-contrast mode at 100 kV accelerating voltage. The samples were prepared by drop casting the solution/dispersion directly on the TEM grids (Ted Pella, 300 mesh, carbon layer) and they were subsequently kept in a box saturated with solvent vapors for 24 h. Finally, the box was slowly flushed with nitrogen for another 24 h, and the samples were dried under vacuum at room temperature for 60 h.

Atomic force microscopy (AFM) data was obtained using a SOLVER Pro-M scanning probe microscope (NT-MDT, Russia). The AFM images were taken in air at room temperature. For the instrument operation, we chose a tapping mode at 255 kHz oscillation mean frequency, using a NSG10/Au Silicon tip, gold covered, with a 10 nm radius of curvature. The images have 256 × 256 scan point size. They were taken with a scan velocity varying from 1 to 6 μm/s depending on the scan area (four-squares with the sides of 20 and 5 μm). In order to distinguish different phases in the sample, a phase contrast mode was used. This technique is specific for the scanning probe microscope. The Nova v.1443 and IA-P9 softwares were used for recording and analyzing the AFM topographic and phase contrast images.

Electrical conductivity of the polymer and nanocomposite samples was measured with a broadband Novocontrol Alpha dielectric spectrometer (Novocontrol Technologies, Germany). For sample preparation, we used a pair of polished brass round plate electrodes which had diameters of 30 and 20 mm. We took 50 mg of the PAZ or PAZ/rGO nanocomposite, put it on the larger plate, heated to the isotropic state (~160 °C), and carefully covered with the preheated smaller plate. To achieve a uniform spread of a melted sample between electrodes, we used silica spacers of diameter of 50 μm. The round plate electrodes filled with the polymer/nanocomposite were then cooled down slowly to room temperature. The measurements were performed at 20 °C and at 1 Hz alternating current frequency.

For rGO conductivity measurements, we used P-8nano and P-30 J potentiostats (Alins, Chernogolovka, Russia). These instruments allow investigating electrical properties of samples by measuring either current vs. applied voltage

(potentiostatic regime) or voltage vs. specified current (galvanostatic regime). The method allows using measuring cells in arrangement with two-, three- or four-electrodes set. A measurement mode depends on construction of a sample-cell system under investigation and requirement of contact resistance accounting on the electrode-sample border. Obtained voltage-current characteristics allow determining sample resistance and calculating its specific conductivity.

Results and discussion

Characterization of rGO nanoparticles

FTIR spectroscopy measurements

FTIR spectra of GO and rGO are shown in Fig. 2. A set of intense bands in the OG spectrum in the range 3000–3700 cm^{-1} is related to oscillations of hydroxyl groups and O-H bonds in absorbed water [28]; the band at 1725 cm^{-1} is related to oscillations of C = O bonds in carbonyl and carboxyl groups (the bands of stretching vibrations of C-OH bonds at 3614 cm^{-1} and O-H bonds at 3216 cm^{-1} are related to carboxyl groups too [28, 29]); the bands at 1612 cm^{-1} and at 3378 cm^{-1} correspond to the bonds oscillation in absorbed (intercalated) water molecules; and the band at 1064 cm^{-1} corresponds to the stretching vibrations of the C–O bonds in alkoxy and epoxy groups [28]. The band at 1336 cm^{-1} refers to hydroxyl groups, particularly to the C-OH bonds oscillation, while the band at 1242 cm^{-1} is related to the C-O-C oscillations of alkoxy and epoxy groups. Hereby, we can conclude that the prevailing GO functional groups are carboxyl, carbonyl, epoxy, and hydroxyl ones [28]. In addition, according to our EDS data, the carbon-oxygen (C/O) ratio in initial GO is about 1.5. This value also indicates a high oxygen content due to the presence of oxygen-containing

functional groups. For this reason, GO is concluded to be a typical insulator. For completely oxidized graphene, the C/O ratio is known to rich ca. 1.3 [30].

As follows from Fig. 2, in the rGO spectrum the bands in the range of 3000–3700 cm^{-1} disappear. This indicates complete water removal and, consequently, the absence of hydroxyl and carboxyl groups. At the same time, in the range of 900–1800 cm^{-1}, three dominant bands at 1740, 1570, and 1210 cm^{-1} could be observed. A weak band at 1740 cm^{-1} corresponds to C = O stretching vibrations in residual carboxyl and carbonyl groups. However, the band at 1570 cm^{-1} indicates the presence of aromatic C = C bounds (in-plane vibrations). The most intensive band at 1210 cm^{-1} with a hard discernible shoulder at 1000–1050 cm^{-1} refers to oscillations of C-O-C bonds in epoxy and alkoxy groups. It could be effectively removed only at continuous annealing of GO at high temperatures (about 1000°C) in inert atmosphere [31]. The FTIR spectra evidence that the GO thermal reduction results in complete water, hydroxyl, and carboxyl groups removing. However, a part of functional groups, as supposed, are transformed into epoxy groups, which finally contains the main quantity of residual oxygen in rGO. As a consequence, the intense broad band at 1210 cm^{-1} is observed in the rGO spectrum. This band corresponds to C-O-C bonds oscillations.

The EDS data confirm considerable decreasing of oxygen content in rGO as compared with that in initial OG. The C/O index of the rGO increases up to ~5.7, and its electrical conductivity increases notably too (see below).

So, it is clear that thermal shock reduction leads to incomplete removal of oxygen-containing functional groups from GO. In fact, the obtained rGO should rather be considered as a partially reduced GO (prGO). Nevertheless, the incomplete GO reduction in not a problem for producing polymer nanocomposites with enhanced conductivity. For example, the PANI-based nanocomposites have been reported [15, 16, 32] to exhibit relatively higher conductivity when/if they contained prGO rather than rGO. The partially oxidized graphene $\pi-\pi$-interactions with PANI due to the presence of functional groups prevent prGO particles aggregation and promote their more uniform distribution in the nanocomposite. As a result, a network of charge-transport paths spreads significantly in nanocomposite film and the charge carriers mobility enhances [15, 16].

UV-Vis spectroscopy measurements

For UV-Vis spectroscopy analysis of OG and rGO, their water dispersions were prepared. OG was simply diluted with additional amount of water. Both GO and rGO dispersions were afterwards subjected to sonication. It should be noted that produced rGO flakes easily forms a stable dispersion due to residual hydrophilic functional groups remained after the incomplete GO reduction. Nevertheless, the rGO water dispersion was stable only for one week whereupon noticeable rGO particles
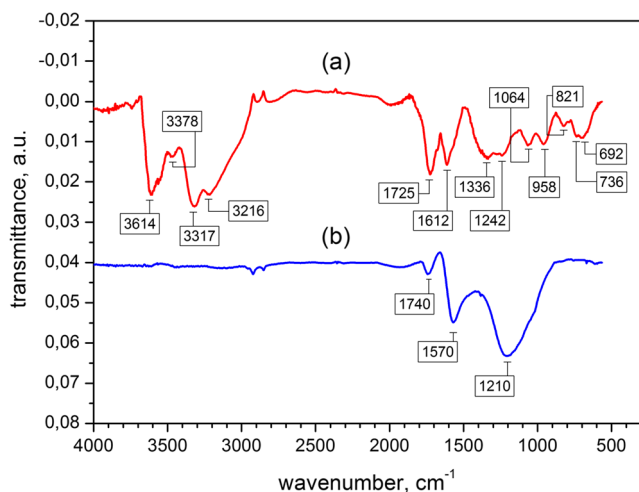
Fig. 2 FTIR spectra of (**a**) GO and (**b**) rGO

sedimentation occurred while rGO dispersion in DMF was quite stable for several months. The photographs of the referred dispersions and a PAZ/DMF solution are presented in Fig. 3.

The UV-Vis spectra of diluted GO and rGO water dispersions are shown in Fig. 4. In the GO spectrum, there are two characteristic absorption regions in the form of peak with a maximum at 232 nm and a shoulder in the region 290-300 nm. The first one corresponds to $\pi–\pi*$ electron transition in the C = C bounds, while the second one corresponds to $n–\pi^*$ electron transition in the C = O bounds in carbonyl groups [33]. After GO reduction, a bathochromic shift from 232 nm to 273 nm of the first maximum occurs, while the shoulder fully disappears [34]. It indicates enough complete carbonyl groups removal [33].

WAXS data analysis

The WAXS data for GO and rGO samples is shown in Fig. 5. In the WAXS spectrum of GO, two peaks could be recognized: the intensive peak at $2\Theta = 10.4°$ and the second one at $2\Theta = 20.4°$, while for rGO only one low intensity peak at $2\Theta = 25°$ could be observed.

The interlayer distance of the GO and rGO stacks could be calculated using the Bragg's law [28, 31].

$$n\lambda = 2d_{hkl}\sin\Theta \qquad (1)$$

where λ is the X-ray wavelength, Θ is the scattering angle, n is an integer representing the diffraction peak order, d is the interlayer distance of lattice, and (hkl) are Miller's indices.

The mean size of stacks could be determined using the Scherrer's eq. [28, 31]

$$L_{hkl} = \frac{k\lambda}{\beta_0\cos\Theta}, \qquad (2)$$

where L_{hkl} is the stacks thickness, β_0 is the full width at the half maximum (FWHM) in radians, K is the stacks shape factor (0.89).
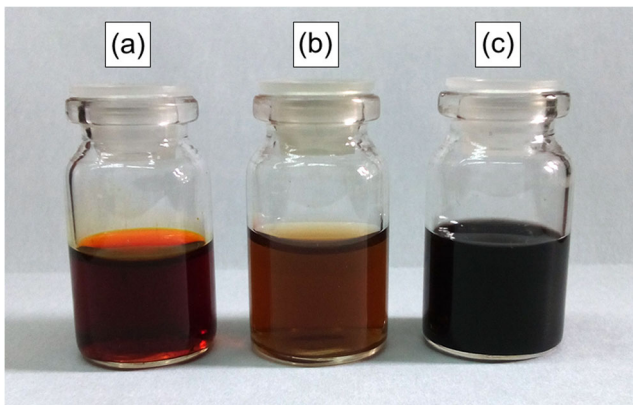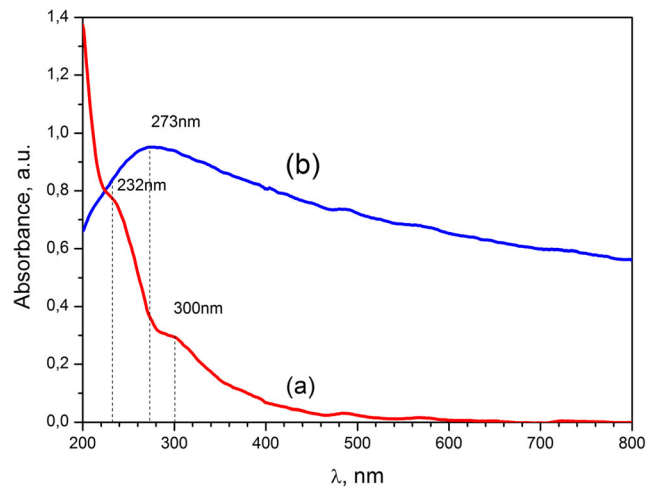
Fig. 4 UV-Vis spectra of diluted (**a**) GO/DMF and (**b**) rGO/water dispersions

Structural parameters of GO and rGO stacks calculated with Eqs. (1) and (2) are presented in Table 1. It could be seen from Table 1 that GO has the maximum interlayer distance d_{002} of lattice due to the presence of a great number of oxygen-containing functional groups and intercalated water molecules. Functional groups in GO are expected to prevent stacks aggregation (or dense packing) because of electrostatic repulsion [16]. At the same time, graphene stacks without functional groups tend to form large aggregates due to strong hydrophobic $\pi–\pi$ interactions [16].

As follows from Table 1, an intensive removal of intercalated water under thermal reduction leads to GO stacks exfoliation and significant decreasing of interlayer distance (from 8.5 to 3.56 Å) in final rGO stacks. If the mean size of GO/rGO stacks is known (it could be calculated with the Scherrer's equation), it is possible to estimate the average number of graphene layers in the stacks. Interestingly, the number of layers in stacks of both GO and rGO samples was found to
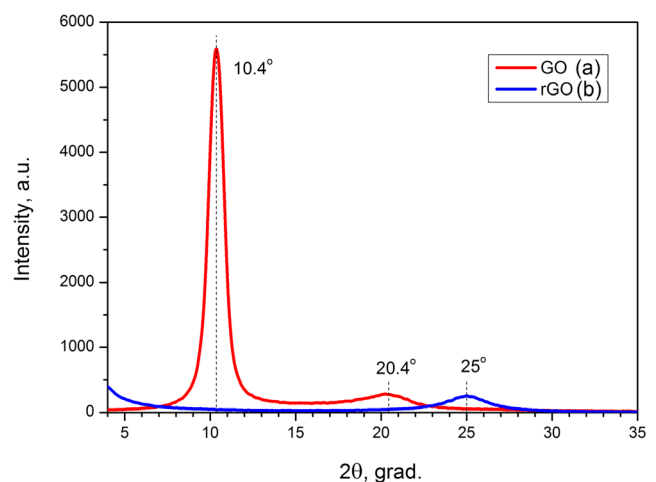
Fig. 3 Photographs of (**a**) of PAZ/DMF solution, (**b**) GO/water dispersion, and (**c**) rGO/DMF dispersion

Fig. 5 WAXS patterns of (**a**) initial GO and (**b**) rGO

Table 1 Structural parameters of GO and rGO obtained from WAXS data and calculated with Eqs. (1) and (2)

Samples	2θ, grad	FWHM, grad (rad)	Interlayer distance d_{002}, Å	Mean size of stacks, Å	Number of layers in stacks
GO	10.4	1.13 (0.0197)	8.50	69.63	~ 8
rGO	25	2.94 (0.0514)	3.56	27.36	~ 8

be equal approximately to 8 (see Table 1). According to Ref. [28], the most intensive intercalated water removal under the thermal reduction occurs at temperature higher than 200 °C, while in the range 500–600 °C the removal of majority of hydroxyl and carboxyl groups occurs. Residual hydroxyl and epoxy groups are removed at temperature above 600–1000 °C. It should be noted, that the GO heating to higher than 1000 °C leads to intensive destruction of aromatic C = C bounds and appearance of a great number of rGO structure defects and drastic decreasing of stacks mean size [31].

According to the data obtained, after GO thermal reduction at 800 °C, a drastic decreasing the peak intensity at $2\Theta = 25°$ and broadening its FWHM are observed. As follows from Table 1, the interlayer distance d_{002} in lattice of rGO is about 3.56 Å. This value is quite similar to that of native graphite (3.4 Å). These facts confirm removal of intercalated water and majority of oxygen-containing functional groups, which prevent layers dense packing in initial GO stacks and good graphene layers exfoliation [13, 16, 31]. We suppose that the monolayer structure of rGO contains some amount of rGO stacks due to the layers packing and folding. At the same time, residual oxygen-containing groups seem to be located essentially on the edges or defects of rGO stacks.

Microscopic data analysis

The SEM- and TEM-images of the rGO nanoparticles are shown in Fig. 6. Both single large-scaled rGO sheets and rGO stacks could be seen on microscopic images. Yet, all of rGO layers could not be clearly recognized because of their folding and overlapping. In the SEM-image (Fig. 6a), the crumpled structure of rGO sheets could clearly be seen. Additionally, the TEM-images evidence different number of layers in the rGO stacks. In Fig. 6b, the nanoparticles vary in their transparency. This means that the stacks contain a different number of graphene layers. A large rGO stack selected in Fig. 6b is shown in Fig. 6c at a higher magnification. The approximate planar size of the rGO particles was estimated from Fig. 6b as 200–1000 nm.

Electrical conductivity measurements

As mentioned above, completely oxidized graphene is known to be either an insulator or a very weak conductor. According to Ref. [7], the rGO surface conductivity is known to vary within a wide range: from a few tens up to three thousands of Cm/m, depending on production method and reduction value. In our study, the rGO conductivity appears to be 35 Cm/m, that is in accordance with the literature data for thermally reduced GO.

Characterization of PAZ and PAZ/rGO nanocomposite

FTIR spectra analysis

The FTIR spectra of pure PAZ and PAZ/rGO nanocomposite are presented in Fig. 7 where characteristic bands are identified and attributed. It is clear that both spectra are principally identical, though intensity redistribution of some minor bands in the nanocomposite spectrum could be recognized in comparison with that of pure PAZ. This finding seems to be associated with a considerable decrease of the doped polymer crystallinity. Since pure PAZ is a copolymer of diamine and dialdehyde [24], it has some residual functional groups at the ends of the polymer chain. As a result, its FTIR spectrum demonstrates some typical peaks in characteristic region 3400–3500 cm^{-1} corresponding to residual amine groups,
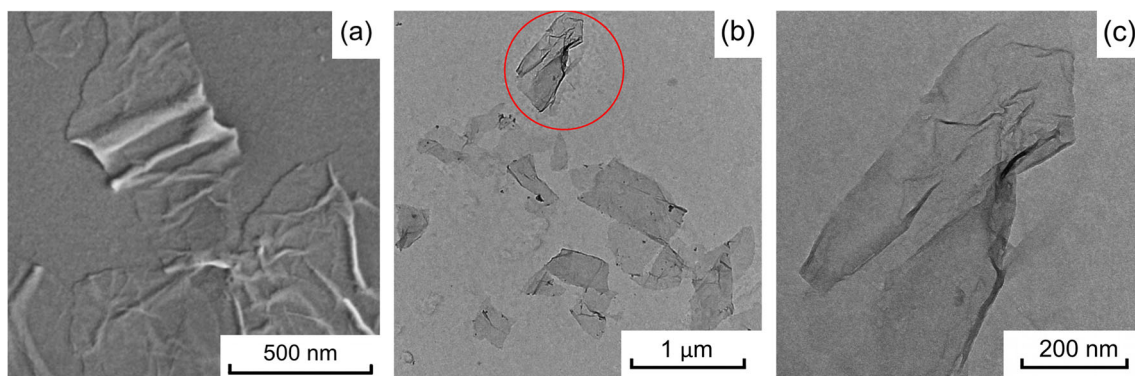
Fig. 6 SEM (**a**) and TEM (**b**, **c**) images of rGO nanoparticles

Fig. 7 FTIR spectra of (**a**) PAZ and (**b**) PAZ/rGO nanocomposite
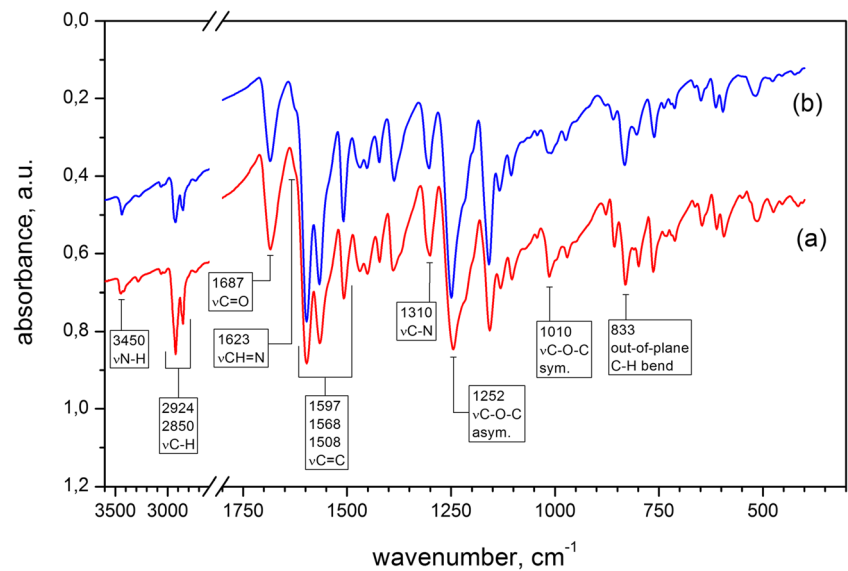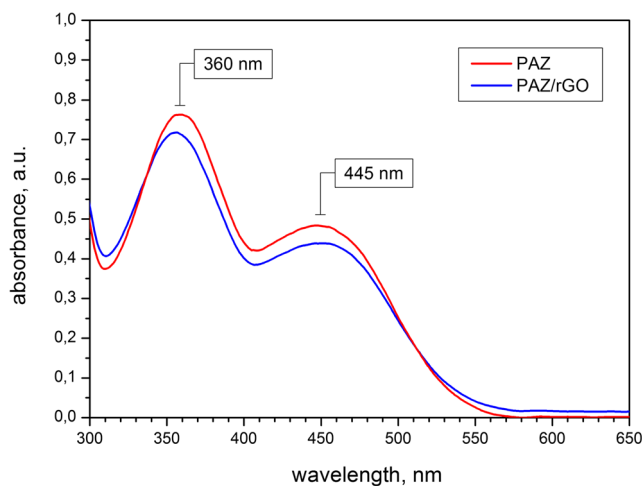

while at 1687 cm^{-1} one can see a weak peak corresponding to oscillations of C = O bounds in residual aldehyde groups.

According to the FTIR spectra, we can conclude that there are no chemical interactions between PAZ and rGO in the nanocomposite.

UV-Vis spectroscopy measurements

In Fig. 8, the UV-Vis spectra of solutions of both pure PAZ and PAZ/rGO nanocomposite in DMF are shown. In the spectrum of the pure polymer, there are two clearly resolved peaks with maxima at 360 and 445 nm. These maxima correspond to π–π* and n–π* electron transitions, respectively [24]. Azobenzene fragments of the polymer macromolecule can exist in either *cis-* or *trans-*isomers. The presence of characteristic absorption bands in the UV-spectrum of PAZ

evidences predominance of *cis-*isomers [35]. At the same time, the spectrum of PAZ/rGO solution exhibits no changes as compared with that of pure polymer. It confirms neither chemical interaction between nanocomposite components nor their complexation.
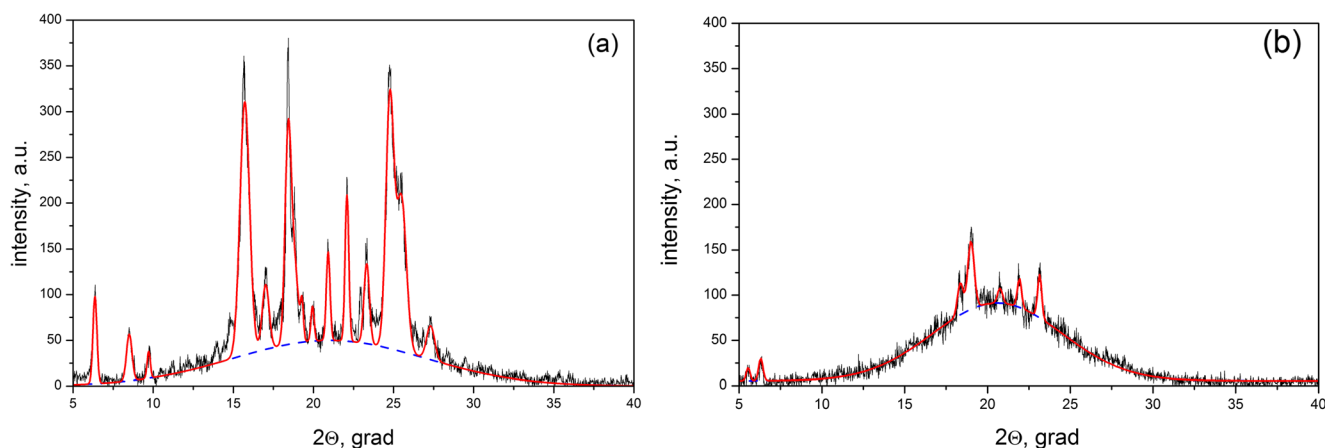
WAXS data analysis

The WAXS patterns of pure PAZ and PAZ/rGO nanocomposite are presented in Fig. 9. In the WAXS pattern of pure polymer, tiny intensive sharp peaks could be observed. This finding indicates high crystallinity of the polymer. At the same time, number and intensity of nanocomposite WAXS pattern peaks decreases significantly. This evidences a decrease in the nanocomposite crystallinity.

Applying a deconvolution technique to the WAXS patterns allows separation of regions (peaks) characterizing contribution of crystal and amorphous fractions in both polymer and nanocomposite samples [36]. For quantitative analysis of polymer and nanocomposite crystallinity, both 'amorphous' and 'crystalline' peaks in the XRD patterns were described using the Gauss distribution and their areas were defined. Crystallinity χ was estimated through relation of summary area of crystalline peaks to total area of difractogram [36]

$$\chi = \frac{I_{cryst}}{I_{cryst} + I_{am}} \times 100\%, \tag{3}$$

where I_{cryst} and I_{am} are the crystalline and amorphous areas, respectively.

According to the WAXS analysis with Eq. (3), the crystallinity of pure PAZ and PAZ/rGO nanocomposite was found to be equal 65 and 10%, respectively. Decreasing of nanocomposite crystallinity in comparison with pure polymer is also confirmed by the results of the SEM analysis (see below).


Fig. 8 UV-Vis spectra of solutions of (1) pure PAZ and (2) PAZ/rGO nanocomposite in DMF

Fig. 9 WAXS patterns of (**a**) pure PAZ and (**b**) PAZ/rGO nanocomposite. Red solid lines indicate the crystalline areas contribution and blue dashed lines indicate the amorphous areas contribution

Microscopic data analysis

The SEM-images of pure PAZ and PAZ/rGO samples are shown in Fig. 10. In the SEM-image of pure PAZ (Fig. 10a), morphological structures in the form of crystallites could be clearly recognized. As could be seen from Figs. 10b and c, when the polymer is loaded with the rGO nanoparticles, its morphology dramatically changes. The crystallites size significantly decreases and become almost indistinguishable in the image presented in Fig. 10c. The composite fracture surface at a less magnification is shown in the Fig. 10b. There are a lot of well recognized both small and large rGO particles emerging to the fracture surface from the nanocomposite volume. It is clear that rGO nanoparticles differ in size and are dispersed almost uniformly in the polymer matrix; they do not form large-scaled aggregates. At the same time, any notable ordering of rGO particles could not be observed: they are not aligned in any direction and allocated both in the plane of fracture surface and at different angles to it. A single rGO particle emerging to the fracture surface is presented in Fig. 10c at a larger magnification.

The TEM-images of PAZ/rGO nanocomposite are shown in Fig. 11. In Fig. 11a one can see a large irregular-shaped single rGO stack with a planar size about 1 μm. Since it exhibits varying transparence, we can conclude that it consists of a few graphene layers. In Fig. 11b, the TEM-image of PAZ/rGO at a less magnification is shown. It is clear that rGO nanoparticles are uniformly distributed in the polymer matrix; their planar size achieves ca. 800–1000 nm.

For detailed nanocomposite morphology analysis, we used the AFM-data. They are presented in Fig. 12. In Fig. 12a and c, the AFM topographic images of the PAZ/rGO nanocomposite for different scan areas are shown. In these images, the surface of the nanocomposite film seems to be quite uniform. Yet, a lot of round-shaped "bulbs" could be recognized on the film surface. According to their size and aspect ratio, these "bulbs" could be attributed to the polymer phase rather than to the rGO nanoparticles. We believe that the "bulbs" would be referred to specific morphological structures/defects arising from non-optimal conditions of PAZ/rGO film formation. The phase contrast images of the different scan
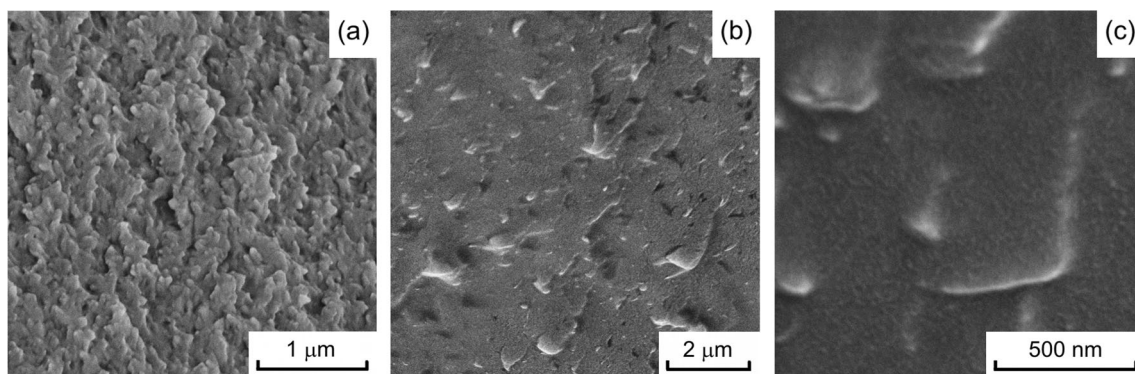
Fig. 10 SEM-images of (**a**) pure PAZ, (**b**) and (**c**) PAZ/rGO nanocomposite

Fig. 11 TEM-images of (**a**) single rGO stack in polymer matrix and (**b**) uniform distribution of rGO stacks in PAZ/rGO nanocomposite
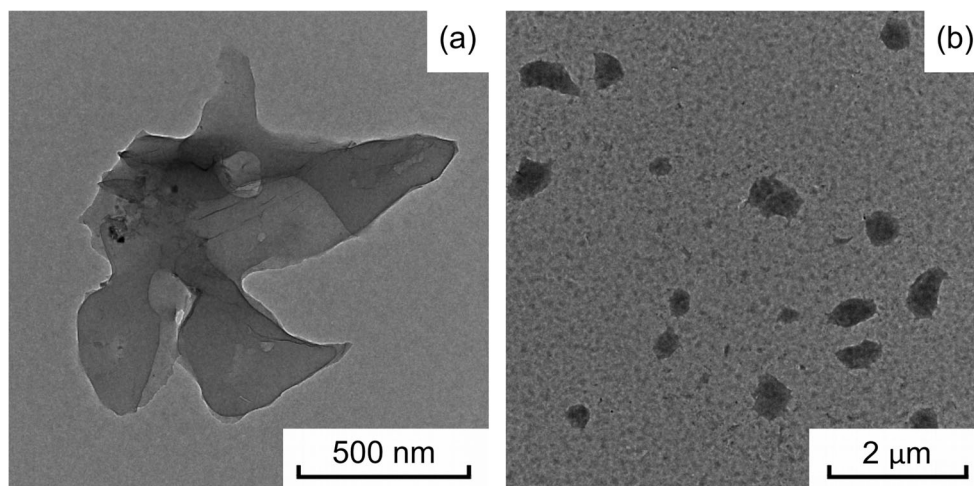
areas are shown in Figs. 12b and d. These areas correspond to those depicted in Fig. 12 a and c, respectively. The rGO nanoparticles are clearly recognized in Fig. 12 b and d in form of solid dark objects. It is evident that rGO nanoparticles are distributed uniformly in the nanocomposite film and covered with a very thin polymer layer.

According to Refs. [7, 8], when layered materials, such as graphene, are used as nanofillers for polymer-based composites, three types of phase separation are possible: stacked, intercalated or exfoliated. When a polymer chain is unable to intercalate between the graphene sheets (because of either insufficient exfoliation of graphite or restacking of layers during reduction of GO), a phases separated composite is formed. It contains large stacked agglomerates of graphene sheets. However, superior properties of nanocomposites can be achieved if there is a strong interfacial interaction between graphene and the polymer matrix. In the exfoliated structure, graphene flakes have the largest possible interfacial contact with the polymer matrix. Assuming the data obtained, we believe that the PAZ/rGO nanocomposite exhibits intercalated type of phase separation because the polymer matrix contains both exfoliated single rGO sheets and rGO stacks with intercalated polymer chains. Besides, decreasing crystallinity of the polymer after its loading with rGO also confirms polymer chains intercalation into the rGO stacks.

*Electrical conductivity measurements*

As mentioned above, the electrical conductivity of PAZ and PAZ/rGO nanocomposite was measured with the BDS technique at room temperature and at the alternating current frequency of 1 Hz. The values of conductivity were found to be equal to 9.2×10^{-13} Cm/cm for pure polymer and 4.2×10^{-9} Cm/cm for the nanocomposite. This means that insulating polymer becomes a semiconducting material after its loading

with rGO. The increased conductivity of the PAZ/rGO composite is in good agreement with literature data for polymer/rGO nanocomposites [3, 7, 8]. Also, earlier we found that PAZ/C_{60} nanocomposite exhibited similar conductivity but at higher dopant loading (2.5 wt%) [22]. Thus, we can conclude that 2-D carbon nanoparticles are more effective for fabrication of polymer nanocomposites with enhanced conductivity as compared with 0-D ones.

Conclusions

We produced rGO by thermal shock reduction of GO followed by its annealing at 800 °C. Then stable rGO dispersion in DMF was fabricated. Using a set of experimental methods (WAXS; FTIR, UV, and BDS spectroscopy; four-probe conductivity method; and XPS), high reduction level of GO and removal the majority of oxygen-containing functional groups was confirmed. It was shown that the C/O ratio increased from 1.5 up to 5.7 during GO reduction. The specific conductivity of rGO was found to be 35 Cm/m. This result proves successful GO thermal reduction. It was revealed that rGO particles form stacks, comprising by approximately 8 graphene layers with a planar size about 200–1000 μm.

The rGO dispersion in DMF was used for producing the conductive PAZ/rGO nanocomposite by solution blending method. The rGO loading in nanocomposite was 2 wt%. According to the SEM, TEM and AFM investigations, the rGO particles are distributed in the polymer matrix uniformly, while neither particles aggregation nor their ordering were found. Besides, a significant decrease in PAZ/rGO crystallinity as compared with pure PAZ was revealed. This indicates strong physical interaction between the composite components. Based on the data obtained, we proposed that PAZ/rGO nanocomposite
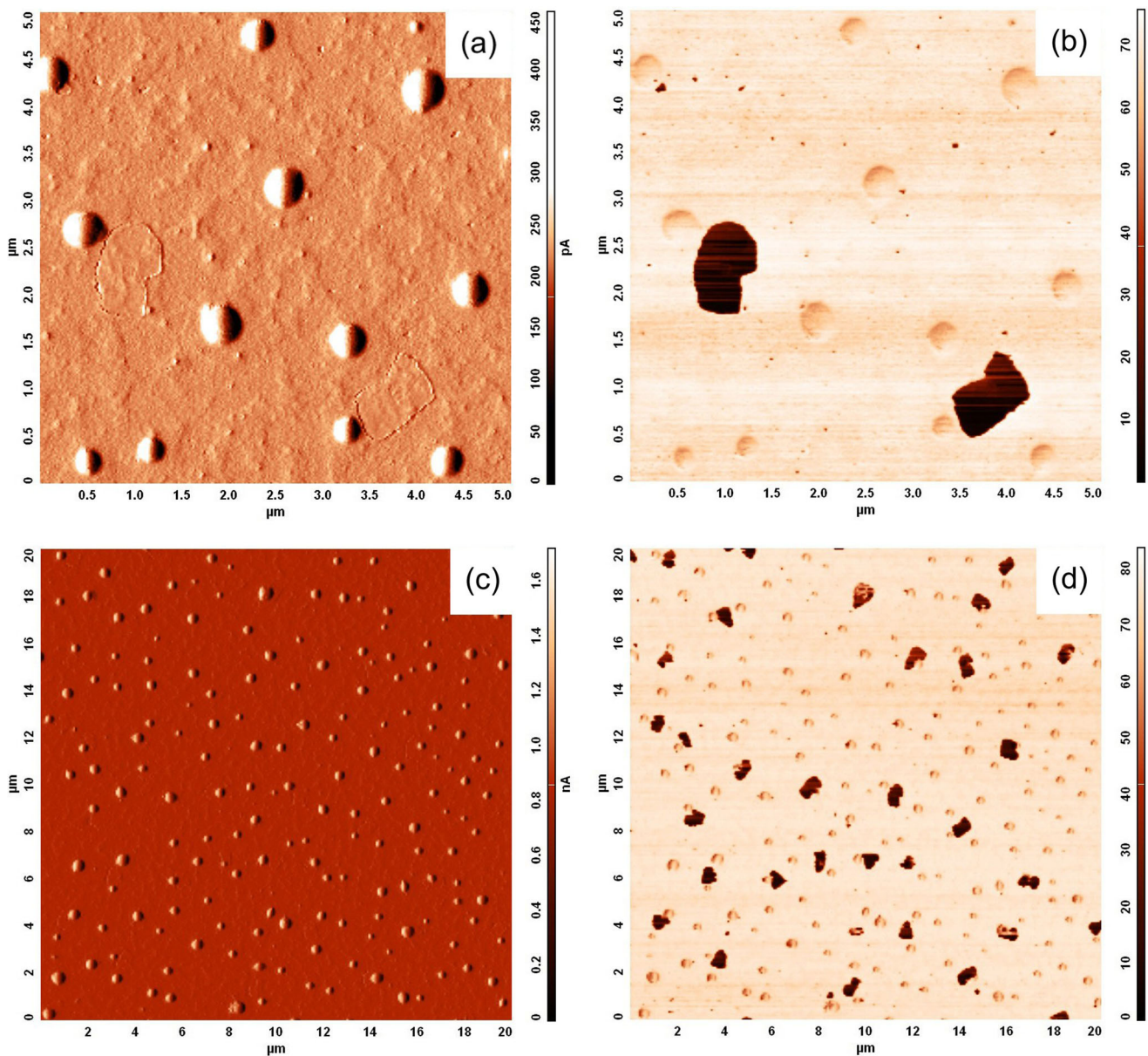
Fig. 12 (**a**) and (**c**) – AFM topographic images; (**b**) and (**d**) – AFM phase contrast images of PAZ/rGO nanocomposite; (**a**) and (**b**) relate to 5 × 5 μm scan area whereas (**c**) and (**d**) relate to 20 × 20 μm scan area

could rather be referred to so-called intercalated phases type [7]. Using the FTIR and UV spectroscopy data, we confirmed the absence of chemical interaction between PAZ and rGO. Electrical conductivity of PAZ and PAZ/ rGO nanocomposite was measured using a BDS method. The electrical conductivity of the nanocomposite was found to increase for four orders as compared with that of neat polymer. Nevertheless according to the TEM- and AFM-data, the percolation conductivity paths in the nanocomposite could not be recognized. As proposed in literature [16], percolation paths in conjugated polymer-based nanocomposites are not necessary for their conductivity. Due to the interaction between conjugated polymer chains and rGO, additional charge transport paths could be formed [16]. As a result, the nanocomposite conductivity increases. Therefore, the data presented in the paper allow us to suppose potential utilizing of conjugated polyazomethines for fabrication of conductive nanocomposites with a small rGO loading.

References

1. Paul DR, Robeson LM (2008) Polymer nanotechnology: Nanocomposites. Polymer 49:3187–3204

2. Jancar J, Douglas JF, Starr FW, Kumar SK, Cassagnau P, Lesser AJ, Sternstein SS, Buehler MJ (2010) Current issues in research on structure-property relationships in polymer nanocomposites. Polymer 51:3321–3343

3. Kuilla T, Bhadra S, Yao D, Kim NH, Bose S, Lee JH (2010) Recent advances in graphene based polymer composites. Progr Polym Sci 35:1350–1375

4. Jariwala D, Sangwan VK, Lauhon L, Marks TJ, Hersam MC (2013) Carbon nanomaterials for electronics, optoelectronics, photovoltaics, and sensing. Chem Soc Rev 42:2824–2860

5. Wang C, Guo Z-X, Fu S, Wu W, Zhu D (2004) Polymers containing fullerene or carbon nanotube structures. Prog Polym Sci 29:1079–1141

6. Badamshina E, Gafurova M (2012) Polymeric nanocomposites containing non-covalently bonded fullerene C60: properties and applications. J Mater Chem 22:9427–9438

7. Phiri J, Gane P, Maloney TC (2017) General overview of graphene: production, properties and application in polymer composites. Mater Sci Eng B 215:9–28

8. Potts JR, Dreyer DR, Bielawski CW, Ruoff RS (2011) Graphene-based polymer nanocomposites. Polymer 52:5–25

9. Shao Y, Wang J, Engelhard M, Wang C, Lin Y (2010) Facile and controllable electrochemical reduction of graphene oxide and its applications. J Mat Chem 20:743–748

10. Low CTJ, Walsh FC, Chakrabarti MH, Hashim MA, Hussain MA (2013) Electrochemical approaches to the production of graphene flakes and their potential applications. Carbon 54:1–21

11. Wang J, Wang X, Xu M, Zhang M, Shang X (2011) Preparation of graphene/poly(vinyl alcohol) nanocomposites with enhanced mechanical properties and water resistance. Polym Int 60:816–822

12. Kashyap S, Pratihar SK, Behera SK (2016) Strong and ductile graphene oxide reinforced PVA nanocomposites. J Alloys Compounds 684:254–260

13. Xie F, Qi SH, Wu D (2016) A facile strategy for the reduction of graphene oxide and its effect on thermal conductivity of epoxy based composites. Express Polym Lett 10:470–478

14. Pron A, Rannou P (2002) Processible conjugated polymers: from organic semiconductors to organic metals and superconductors. Progr Polym Sci 27:135–190

15. Omelchenko OD, Gribkova OL, Tameev AR, Vannikov AV (2014) The effect of the degree of graphene oxidation on the electric conductivity of nanocomposites based on a polyaniline complex. Tech Phys Lett 40:807–809

16. Iakobson OD, Gribkova OL, Tameev AR, Kravchenko VV, Egorov AV, Vannikov AV (2016) Conductive composites of polyaniline–polyacid complex and graphene nanostacks. Synth Metals 211:89–98

17. Imran SM, Kim Y, Shao GN, Hussain M, Choa Y, Kim HT (2014) Enhancement of electroconductivity of polyaniline/graphene oxide nanocomposites through in situ emulsion polymerization. J Mater Sci 49:1328–1335

18. Solonaru AM, Grigoras M (2017) Water-soluble polyaniline/graphene composites as materials for energy storage applications. Express Polym Lett 11:127–139

19. Iwan A, Sek D (2008) Processible polyazomethines and polyketanils: from aerospace to light-emitting diodes and other advanced applications. Prog Polym Sci 33:289–345

20. Hussein MA, Abdel-Rahman MA, Asiri AM, Alamry KA, Aly KI (2012) Review on liquid crystalline polyazomethines polymers: basics, syntheses and characterization. Designed monomers. Polymers 15:431–463

21. Bronnikov S, Kostromin S, Musteaţa V, Cozan V (2015) Polyazomethine with m-tolylazo side groups: thermal, dielectric and conductive behaviour. Liq Cryst 42:1102–1110

22. Bronnikov S, Podshivalov A, Kostromin S, Asandulesa M, Cozan V (2017) Electrical conductivity of polyazomethine/fullerene C60 nanocomposites. Phys Lett A 381:796–800

23. Bronnikov S, Kostromin S, Musteaţa V, Cozan V (2016) Dielectric study of side-chain liquid crystalline polyazomethine/fullerene C60 nanocomposite. J Polym Res 23:54

24. Cozan V, Iftime M, Sava I, Bronnikov S (2015) Synthesis and thermotropic properties of polyazomethines containing side chain azobenzene moieties. High Perform Polym 27:661–668

25. Hummers WS, Offeman RE (1958) Preparation of graphitic oxide. J Am Chem Soc 80:1339–1339

26. Punetha VD, Rana S, Yooc HJ, Chaurasiad A, McLeskey JT, Ramasamy MS, Sahoo NG, Cho JW (2017) Functionalization of carbon nanomaterials for advanced polymer nanocomposites: a comparison study between CNT and graphene. Prog Polym Sci 67:1–47

27. Yin H, Dittrich B, Farooq M, Kerling S, Wartig K-A, Hofmann D, Huth C, Okolieocha C, Altstädt V, Schönhals A, Schartel B (2015) Carbon-based nanofillers/poly(butylene terephthalate): thermal, dielectric, electrical and rheological properties. J Polym Res 22:140

28. Seresht RJ, Jahanshahi M, Rashidi AM, Ghoreyshi AA (2013) Synthesis and characterization of thermally-reduced graphene. Iranica J Energy Environ 4:53–59

29. Acik M, Lee G, Mattevi C, Chhowalla M, Cho K, Chabal YJ (2010) Unusual infrared-absorption mechanism in thermally reduced graphene oxide. Nature Mater 9:840–845

30. Zhang C, Dabbs DM, Liu L-M, Aksay IA, Car R, Selloni A (2015) Combined effects of functional groups, lattice defects, and edges in the infrared spectra of graphene oxide. J Phys Chem C 119:18167–18176

31. Huh SH (2011) Thermal reduction of graphene oxide. In: Mikhailov S (ed) Physics and applications of graphene – experiments. InTech Europe, Rijeka, Croatia, pp 73–90

32. Omelchenko OD, Gribkova OL, Tameev AR, Novikov SV, Vannikov AV (2014) Thin nanocomposite layers based on a complex of polyaniline and graphene. Protect Metals Phys Chem Surf 50:613–619

33. Peng X-Y, Liu X-X, Diamond D, Lau KT (2011) Synthesis of electrochemically-reduced graphene oxide film with controllable size and thickness and its use in supercapacitor. Carbon 49:3488–3496

34. McDonald MP, Morozov Y, Hodak JH, Kuno M (2015) Spectroscopy and microscopy of graphene oxide and reduced graphene oxide. In: Gao W (ed) Graphene oxide. Reduction recipes, spectroscopy, and applications. Springer, Heidelberg, pp 29–60

35. Merino E, Ribagorda M (2012) Control over molecular motion using the cis–trans photoisomerization of the azo group. Beilstein J Org Chem 8:1071–1090

36. Purohit PJ, Huacuja-Sanchez JE, Wang D-Y, Emmerling F, Thünemann A, Heinrich G, Schönhals A (2011) Structureproperty relationships of nanocomposites based on polypropylene and layered double hydroxides. Macromolecules 44:4342–4353